ResearchGate

See discussions, stats, and author profiles for this publication at: https://www.researchgate.net/publication/242015268

Effects of Drop Size and Viscosity on Spreading Dynamics in DC Electrowetting

ARTICLE *in* LANGMUIR · JUNE 2013

Impact Factor: 4.46 · DOI: 10.1021/la401801u · Source: PubMed

CITATIONS
14

READS
53

5 AUTHORS, INCLUDING:

Young Kwon Kim
Pohang University of Science and Technology
7 PUBLICATIONS **21** CITATIONS
SEE PROFILE

Hyoung Kang
TubeBox
45 PUBLICATIONS **178** CITATIONS
SEE PROFILE

Jung Min Oh
IBS Center for Soft and Living Matter
24 PUBLICATIONS **445** CITATIONS
SEE PROFILE

In Seok Kang
Pohang University of Science and Technology
89 PUBLICATIONS **1,225** CITATIONS
SEE PROFILE

Available from: Jung Min Oh
Retrieved on: 01 February 2016

Langmuir

Article

pubs.acs.org/Langmuir

Effects of Drop Size and Viscosity on Spreading Dynamics in DC Electrowetting

Jiwoo Hong,[†] Young Kwon Kim,[†] Kwan Hyoung Kang,[†] Jung Min Oh,*[,‡] and In Seok Kang*[,‡]

[†]Department of Mechanical Engineering and [‡]Department of Chemical Engineering, Pohang University of Science and Technology, San 31, Hyoja-dong, Pohang 790-784, South Korea

Supporting Information

ABSTRACT: This study investigates the effects of drop size and viscosity on spreading dynamics, including response time, maximum velocity, and spreading pattern transition, in response to various DC voltages, based on both experiment and theoretical modeling. It is experimentally found that both switching time (i.e., time to reach maximum wetted radius) and settling time (i.e., time to reach equilibrium radius) are proportional to 1.5th power of the effective base radius. It is also found that the maximum velocity is slightly dependent on drop size but linearly proportional to the electrowetting number. The viscosity effect on drop spreading is investigated by observing spreading patterns with respect to applied voltages, and the critical viscosity at which a spreading pattern changes from under- to overdamped response is obtained. Theoretical models with contact angle hysteresis predict the spreading dynamics of drops with low and high viscosities fairly well. By fitting the theoretical models to experimental results, we obtain the friction coefficient, which is nearly proportional to 0.6th power of viscosity and is rarely influenced by applied voltage and drop size. Finally, we find that drop viscosity has a weak effect on maximum velocity but not a clear one on contact line friction.

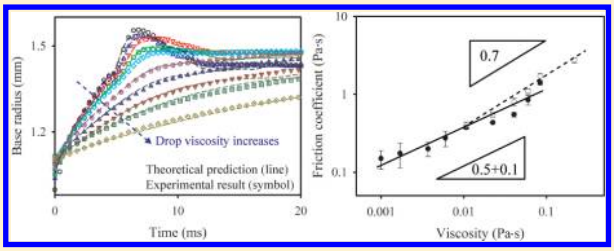

1. INTRODUCTION

The wettability of a drop on an insulator-coated electrode surface can be changed by externally applying a DC or an AC electrical potential. This phenomenon is called electrowetting (EW). EW has many advantages including fast and precise control of contact angle with a low driving voltage. Thus, EW has attracted considerable attention, and many EW-based applications have been developed, including digital microfluidics,[1] liquid lens,[2] microswitches,[3] optical valves and mirrors,[4,5] and reflective displays.[6]

To improve the performance of such devices, a solid understanding of the spreading dynamics of a drop activated by wettability change is crucial.[7] The spreading dynamics in EW can be determined by the balance between the driving electrical force and resistance forces. When an electric field is applied, the electrical force concentrated near the three-phase contact line (TCL) pulls the fluid element near the TCL outward, and this initiates the spreading motion. There are two main resistance forces against the driving electrical force at the TCL: the contact line (CL) friction and the pinning force. The CL friction originates from the molecular displacements near CL and acts as dynamic friction between a drop (or liquid) and a solid plane.[8,9] And the pinning force is manifested by contact angle hysteresis (i.e., CAH, the difference between advancing and receding angles) caused by heterogeneities on solid surfaces.[10]

The movement of the CL induces oscillations on the drop surface, whose shape is determined by a balance between inertia, surface tension, and viscous forces in the bulk. And, at the same time, CL friction on the solid plane plays a role as a resistant force together with viscous dissipation in the bulk. The aforementioned forces are correlated with physical properties such as drop size, viscosity, and surface tension, all of which are important physical parameters influencing the spreading dynamics. For instance, the response time, the maximum velocity, and shape oscillation of the drop surface are observable phenomena affected by combinations of the aforementioned factors. To predict spreading dynamics in EW accurately, studies on how each force mentioned above affects spreading dynamics, and the identification of dominant forces, are required. The problem is that it is hard to separate all effects independently in an experiment.

Some studies have been reported the relationship between physical properties and spreading dynamics, but they are not all consistent. Drop size, which is closely related to the dimensions of EW-based devices, has a direct effect on response time and speed. Smith et al.[11] roughly obtained a linear relationship between drop size and settling times (i.e., time to reach equilibrium radius) in a water−oil system. To clearly determine this relationship, further systematic research is required. Studies on the effects of applied voltage on response time and maximum velocity were also reported. Dash et al.[12] experimentally explored the transient response of a drop in air by DC EW and found that switching time (i.e., the time to

Received: May 11, 2013
Revised: June 24, 2013
Published: June 25, 2013

 © 2013 American Chemical Society

reach maximum wetted radius) is independent of applied voltage. Sen and Kim[13] empirically obtained a linear relationship between the maximum velocity and the applied voltage. On the other hand, Annapragada et al.[14] theoretically predicted a quadratic dependence of the maximum velocity on the applied voltage, which contradicts Sen and Kim's result.[13] The voltage dependence on the maximum velocity has not been clarified in experiments and it will be examined in this work.

Drop viscosity, which can vary practically with different additives such as colorants and reagents, also changes the spreading pattern and eventually affects the response time and speed of EW-based devices.[2,15−17] Kuiper and Hendriks[2] suggested an empirical formula to predict the critical viscosity for the critically damped oscillation of liquids in a cylindrical tube under single DC voltage. However, a study on the applied voltage dependence of the critical viscosity has yet to be reported. Here, we will focus on the influence of drop size and viscosity on spreading dynamics under various DC EW, since these properties can be easily handled in experiment, and the relative strength of inertia, resistance, and electrical forces can be controlled and these are the main control parameters to manipulate microfluidic devices. Other control parameters, such as surface tension and dielectric layer thickness, are practically limited in varying their values.

When it is difficult to correlate physical properties with observable phenomena, theoretical models may guide us in the right direction for explaining spreading dynamics. For predicting spreading dynamics in EW, a few theoretical models have been developed.[12,13] Note that there is no comprehensive model covering the entire range of physical properties in various situations. Decamps and De Coninck[18] proposed a simple mathematical model to predict the spreading dynamics of a drop in air, based on molecular kinetic theory, considering the EW effect. By comparing theoretical and experimental results, they found that the friction coefficient in the dynamic contact angle model is independent of the applied voltage. However, their model could only predict spreading pattern with an overdamped response (i.e., the drop spreads monotonically to its equilibrium configuration without overshoot), since they did not consider the inertia effect. Wang and Jones[19] also developed a theoretical model to predict the transient dynamics of liquid rise between vertically oriented parallel electrodes. By fitting their model to experimental results, they found that the friction coefficient is correlated to liquid viscosity. However, they did not establish the relationship between friction coefficient and viscosity since they were using a limited range of liquid viscosity. Recently, Kang's group developed a theoretical model[20] to predict the spreading dynamics of a weakly viscous drop in air by using the domain perturbation method[21−23] and the dynamic contact angle model[24] considering CL friction and CAH. The model predicts the spreading dynamics of drops with both under- and overdamped response fairly well. However, they did not confirm to what extent theoretical model can predict the spreading dynamics (e.g., drop with different sizes and viscosities).

In this work, we'd like to resolve some inconsistencies reported in early works and clarify the effects of physical properties on spreading dynamics by EW. In particular, we concentrate systematically on the effects of the size and viscosity of a drop in air on spreading dynamics under various step responses, based on experiments together with theoretical analysis. Note that we focus on different aspects to explore the effects of drop size and viscosity on spreading dynamics, respectively. For investigating drop size effects, response time and the maximum velocity of spreading drops for various drop sizes are measured at different voltages. Then, these results are compared with the theoretical models. For investigating viscosity effects, the spreading pattern transition from under- to overdamping is carefully examined to determine the critical viscosity. Then, the relationship between the viscosity and the friction coefficient in the theoretical models is examined in depth. To the best of our knowledge, this is the first detailed study of viscosity dependence on the spreading pattern and friction coefficient of drops over a broad range of viscosities (1−219 mPa·s) under various step responses.

2. EXPERIMENTAL SETUP

The experimental setup used in this study is typical for EW experimentation (Figure 1a).[20,25] Mixtures of water, glycerol, and

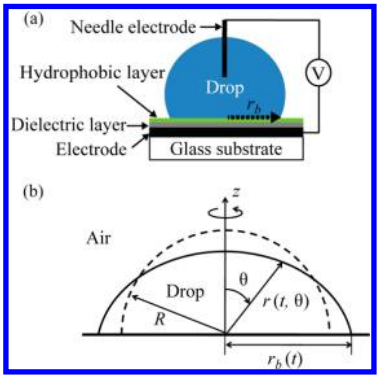

Figure 1. (a) Schematic diagram of the experimental setup. (b) Conceptual description of Oh et al.'s model.[20]

NaCl (1 mM) were used to vary the viscosity of a drop. Indium tin oxide (ITO) electrode plate coated with a dielectric layer (Parylene-C of 5 μm thickness) and a hydrophobic layer (DuPont, AF1600 of 100 nm thickness) and a stainless steel wire of 80 μm in diameter were used as bottom- and top-electrodes, respectively. DC electrical signals, produced by a function generator (33220A, Agilent) and then amplified (A800, FLC), were applied between a wire and an electrode plate. In this work, the EW number η ranging from 0.25 to 0.76, where $\eta = \varepsilon_i\varepsilon_o V^2/2d\gamma$ (i.e., the ratio of the electrical force to the surface tension; ε_i, dielectric constant of insulator; ε_o, vacuum dielectric permittivity; V, applied voltage; d, thickness of insulator; and γ, surface tension of liquid) was used, corresponding to electrical voltages of 80−140 V. Drop size was controlled using a micropipet, and the drops' initial base radii ranged from 0.45 to 1.31 mm, corresponding to volumes of 0.5−10 μL of aqueous 1 mM NaCl solution. In order to minimize gravitational effect, we kept the drop size below capillary length, which is a length scale that represents the relative strength of gravity and surface tension (about 2.7 mm for water). The viscosity of the liquid was varied from 1.01 to 219 mPa·s by increasing the amount of glycerol from 0 to 90 wt %. When the amount of glycerol is larger than 90 wt %, it is difficult to dispense a drop from a pipet tip. The corresponding variations in surface tension and density remain relatively small. The viscosity of the liquids was measured on a rotating viscometer (Brookfield DV-II+ Pro) and surface tension was measured by a Du Noüy ring tensiometer (Lauda TD2). In this experiment, the CAH was in 10 ± 3° regardless of the drop viscosity, which was measured by contact angle meter (Femtofab, SmartDrop SD110TEZ) based on the tilting base method.[26] The measured values of the fluid properties agreed well with the values previously reported.[15,27,28] The physical properties of the working fluids are summarized in Table 1. The deformation process of each drop was recorded using a high-speed camera (Fastcam SA3, Photron) at 10 000−20 000 fps, depending on the CL speed. Image processing and

dx.doi.org/10.1021/la401801u | Langmuir 2013, 29, 9118−9125

Table 1. Physical Properties of the Working Fluids (23 ± 1 °C)

percentage of glycerol (wt %)	viscosity μ (mPa·s)	surface tension γ (dyn/cm)	density ρ (g/cm^3)	Young's angle θ_Y (°)
0	1.0	71.2	0.99	118
20	1.7	68.5	1.05	116
36	2.7	67.3	1.09	114
40	3.7	65.9	1.10	113
46	4.8	65.5	1.12	113
50	6.0	65.2	1.13	112
60	10.7	64.8	1.16	112
64	13.7	64.6	1.16	112
70	22.5	64.5	1.18	111
76	40.6	64.4	1.20	111
80	60.0	64.3	1.21	110
84	84.3	64.3	1.22	110
90	219.0	64.3	1.24	110

data analysis were performed using MATLAB. Every experiment was repeated at least five times, and all presented data were the averaged values of the results. The experimental uncertainties in the contact angle and contact radius measurements are ±2° and ±0.02 mm, respectively. In order to ensure negligible evaporation and absorption and that the drop volume remained constant during the spreading process, the duration of each experiment was limited to a few seconds.

3. RESULTS AND DISCUSSION

3.1. Drop Size Effects. In order to quantify the effects of drop size on the spreading dynamics of drops, we measured the base radius (r_b) (as designated in Figure 1b) of each spreading drop that had initial base radii ranging from 0.45 to 1.31 mm, at different voltages (Figure 2). We compared the apparent contact angle calculated from the base radius in the equilibrium of Figure 2 with that obtained from the Young−Lippmann equation (Supporting Information, Figure S1). Under our experimental conditions, the change in the apparent contact angle was well characterized by the Young−Lippmann equation regardless of drop size. A drop is supposed to be sufficiently small so that a damping effect such as viscous dissipation becomes dominant, rather than the effect of inertia, and so that the transition of a spreading pattern from under- to overdamped response can eventually occur. Unfortunately, the variation of drop size was limited due to our experimental limitations, such as the controlled drop size of micropipet and usage of needle electrode. A spreading pattern transition from under- to overdamped response was observed when the applied voltage increased. At η = 0.25 and 0.39 (80 and 100 V), drops reached their equilibrium state in almost all sizes without overshoot (i.e., overdamped response). When the applied voltage was higher than η = 0.56 (120 V), drops spread with overshoot (i.e., under-damped response). Also, it was observed that the base radius is suddenly increased before the overshoot. This is because the capillary wave, generated at the CL, propagates along the drop surface from the CL to the apex of the drop and subsequently is reflected back toward the CL. This phenomenon is called a kink.[20] In addition, we could see that the peaks of a larger drop in an under-damped response occur later; that is, a smaller drop reaches its maximum peak and equilibrium value faster than a larger drop. From this, we can postulate that the higher voltage increases the driving force, which could influence the development of drop pattern from the overdamped to under-damped response.

The postulation can be justified with a theoretical model. In our previous works, the shape mode equations were derived to describe the unsteady motions of a sessile drop actuated by EW.[20] Here, we do not explain the derivation of the model; details can be found in Oh et al.'s paper.[20] We assumed that the drop shape was only slightly distorted from the hemispherical

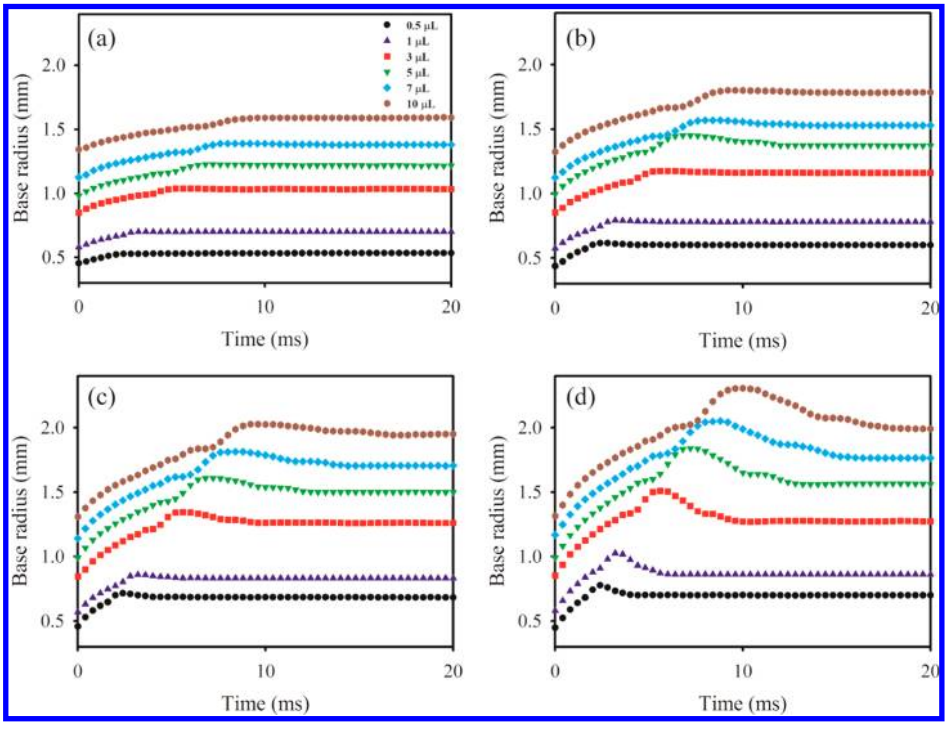

Figure 2. Time evolution of the base radius (symbol) for spreading drops with volumes ranging from 0.5 to 10 μL at different η: (a) 0.25, (b) 0.39, (c) 0.56, and (d) 0.76.

dx.doi.org/10.1021/la401801u | Langmuir 2013, 29, 9118−9125

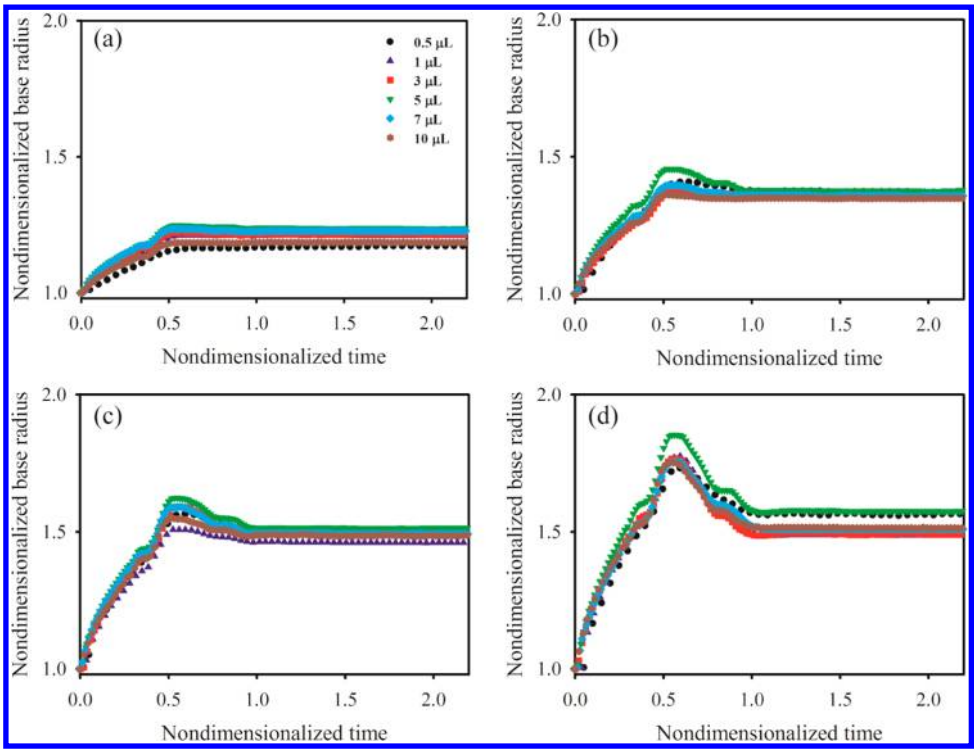

Figure 3. Rescaling the plot of Figure 2 by the period of natural oscillation for the P_2 shape mode and the initial radius at different η: (a) $\eta = 0.25$, (b) $\eta = 0.39$, (c) $\eta = 0.56$, and (d) $\eta = 0.76$. All the cases collapse to one curve along the time axis. For under-damped response, the time to peak and the equilibrium almost correspond to a half, and one period, of natural oscillation for the P_2 shape, respectively.

shape, so the domain perturbation method was used (Figure 1b).[21−23] Drop shape is represented by Legendre polynomial expansion as $F \equiv r - R - \varepsilon\sum_{n=2}^{\infty} a_n(t)P_n(\cos\theta)(F$, shape function; $R = [3\Delta/(2\pi)]^{1/3}$, effective radius; Δ, drop volume; a_n, amplitude of a shape mode; P_n, Legendre polynomial of order n; ε, smallness of drop deformation from the hemispherical shape). The governing equation for shape modes is given by

$$\ddot{a}_n + 2\left[(n-1)(2n+1) + n\frac{\lambda}{\mu}A_{nn}\right]\frac{\mu}{\rho R^2}\dot{a}_n + n(n-1)(n+2)\frac{\gamma}{\rho R^3}a_n = \frac{n(2n+1)}{\varepsilon}\frac{P_n(0)}{\rho R^2}\left[\frac{\varepsilon_d V^2}{2d} + \gamma\cos\theta_Y - c_{pin}sign(U) + \frac{c_{pin}}{\pi/2}\arctan\left(\frac{\lambda}{c_{pin}/(\pi/2)}U\right)\right] - \frac{2n\lambda}{\rho R^2}\sum_{k=2,k\neq n}^{\infty} A_{nk}\dot{a}_k \quad (1)$$

Here, $P_n(0)$ represents a specific shape mode of the drop at the CL. The terms in the bracket on the right-hand side (RHS) of eq 1 represent the dynamic contact angle model that we used,[24] including electrical wetting tension, the capillary force, the pinning force (c_{pin}) induced by CAH, and the nonlinear part of CL friction. The last term (summation term) in the RHS represents the effect of coupling of the other shape modes due to the CL friction, which is proportional to CL velocity (U) with the friction coefficient (λ). Here, A_{nk} represents the coefficient derived from the nonlinear coupling of the shape modes ($k \neq n$) due to the CL friction.[20] A_{nn} ($k = n$) means that there is no interaction between the shape modes. A_{nn} is also dependent on a shape mode. By fitting this model to the experimental results, we obtain the friction coefficients ranging from 0.1−0.2 Pa·s, which rarely have an influence on drop size and applied voltage (Supporting Information). Previous works reported similar results, that the friction coefficient has a weak dependence on the applied voltage.[18−20]

We can generalize spreading dynamics by nondimensionalizing the experimental results in Figure 2. In this problem, the characteristic length scales to the initial base radius ($r_{b,init}$). Neglecting the interaction between shape modes coupled by CL friction (i.e., $k = n$ in eq 1), the shape mode equation (eq 1) can be treated as a second-order linear differential equation governing a mass-spring-damper system. The damped oscillation period, τ_d, for the step input,[29] can be derived as follows:

$$\tau_d = \frac{1}{\sqrt{1-\zeta^2}}\tau_n \quad (2)$$

where

$$\tau_n = 2\pi\sqrt{\frac{\rho R^3}{n(n-1)(n+2)\gamma}},$$

$$\zeta = \left[\frac{(2n+1)}{n(n+2)}\mu + \frac{A_{nn}}{(n-1)(n+2)}\lambda\right]\sqrt{\frac{n(n-1)(n+2)}{\rho R\gamma}}$$

Here, the damping ratio ζ corresponds to the Ohnesorge number (Oh), which is a dimensionless number representing the ratio of the viscous and frictional forces to the inertial and surface tension forces. As aforementioned, the friction coefficients have values ranging from 0.1 to 0.2 Pa·s, so that

dx.doi.org/10.1021/la401801u | Langmuir 2013, 29, 9118−9125

Table 2. Comparison of the Time to Reach Peak Obtained from the Experiments and Calculated Half Periods of Natural Oscillation Using the Effective Radius, Initial Base Radius, and Curvature Radius

	time to reach peak from the experiments, ms				half periods of natural oscillation (n = 2), ms		
drop volume, μL	η = 0.25	η = 0.39	η = 0.56	η = 0.76	Effective radius	Initial base radius	Initial curvature radius
0.5	2.4	2.8	2.4	2.4	2.0	1.2	1.5
1.0	3.0	3.4	3.0	3.4	2.9	1.8	2.1
3.0	5.0	5.6	5.4	5.6	4.9	3.2	3.8
5.0	6.8	6.8	7.0	7.2	6.4	4.1	4.8
7.0	7.6	8.2	8.6	8.6	7.6	5.0	5.9
10.0	9.0	9.4	9.2	9.8	9.0	6.3	7.4

the ratio of the viscous and frictional forces to the inertia and surface tension forces is small (Oh have values ranging from 0.2 to 0.3). Thus, the damped oscillation period is close to the natural oscillation period τ_n of potential flow.[22,23] The period of natural oscillation τ_n for a P_2 shape mode, which is dominant in most cases, can be used as the characteristic time scale. When time and length are nondimensionalized by the period of natural oscillations (i.e., $\tau_n = 2\pi[\rho R^3/n(n-1)(n+2)\gamma]^{0.5}$) for a P_2 shape mode and an initial base radius, respectively, all the cases collapse to one curve along the time axis (Figure 3). For under-damped response, the time to peak and the equilibrium almost correspond to a half, and one period, of natural oscillation for the P_2 shape, respectively. The collapse in Figure 3 shows that the response time is mainly determined by the period of natural oscillation for the P_2 shape mode, and both switching time and settling time are proportional to 1.5th power of the effective base radius. These times are also independent of η. Dash et al.[12] reported a similar result that time to reach a maximum wetted diameter is independent of an applied voltage. Thus, this relationship can help predict the response time when EW-based devices require the drop size to be varied.

The time to reach peak obtained from the experiments was compared with the half periods of natural oscillation calculated from eq 1, using the effective radius, initial base radius, and curvature radius (Table 2). The calculated half period of natural oscillation using the effective radius is almost equal to the time to peak. This may be because drop shape is slightly distorted from the hemispherical shape.

The maximum velocity of spreading drops can represent the upper limit of the response speed of EW-based devices. Sen and Kim[13] experimentally demonstrated that the maximum velocity is linearly proportional to applied voltage, which was also derived from the force balance between inertial and electrical forces. However, they did not consider CL friction. Most recently, Annapragada et al.[14] numerically and theoretically showed that the maximum velocity is proportional to the square of applied voltage. Contact line velocity is maximized at the early stage of spreading (0.2–0.4 ms). At this stage, the inertial force is small because the mass displaced from the original drop is negligible. Thus, the maximum velocity is determined by the balance between CL friction and electrical force. Unfortunately, they could not compare their numerical results with their experimental results. The time to reach the maximum velocity was measured to be from 0.2 to 0.4 ms regardless of drop size and applied voltage, but they conducted experiments with an insufficient image recording rate (1000–2000 fps). We empirically determined that the nondimensionalized maximum velocity was linearly proportional to η and generally became saturated when η is higher than 0.56 (Figure 4). Here, the maximum velocity is nondimensionalized by the capillary velocity ($U_{ca} = \gamma/\lambda$) derived from the balance between capillary force and CL friction.

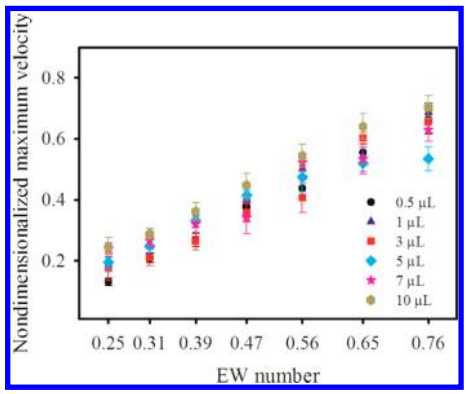

Figure 4. Linear relationship between nondimensionalized maximum velocity and η for spreading drops with different volumes ranging from 0.5 to 10 μL.

3.2. Drop Viscosity Effects. We observed the spreading behaviors of 5 μL drops with various viscosities at different η ranging from 0.25 to 0.76. The shape deformation of spreading drops with low and high viscosities is shown in Figure 5. When the drop has a low viscosity (Figure 5a), the drop spreads quickly when an electrical signal is applied, and almost immediately forms an acute dynamic contact angle within 1 ms. During the initial stages of drop spreading, the capillary wave generated at the CL propagates along the drop surface from the CL to the apex of drop. When the drop has a high viscosity (Figure 5b), it maintains an obtuse dynamic contact angle. In this case, the drop spreads as the shape retains a spherical cap without the capillary wave. Drops with different viscosities have slightly different base radii at 50 ms (Figure 5). This is because the initial base radii (or contact angles) of drops are different due to slight variations in the surface tension depending on viscosity (see Table 1). Two patterns of the spreading process, under- and overdamped oscillations, in respect to viscosity were also observed.

In order to quantify the effects of viscosity on spreading dynamics, the drops' base radii were measured (Figure 6). For convenience, the base radius is nondimensionalized by the initial base radius ($r_{b,init}$) rather than the volume averaged radius. As mentioned before, two different spreading patterns were observed. As the viscosity of a drop increases, the damping effect due to viscous dissipation and friction becomes greater. When the damping effect is larger than the inertial effect, a transition spreading pattern from under- to over-damped response occurs. Critical viscosities (μ_c) for transition between the two patterns measured in experiments are about

dx.doi.org/10.1021/la401801u | Langmuir 2013, 29, 9118–9125

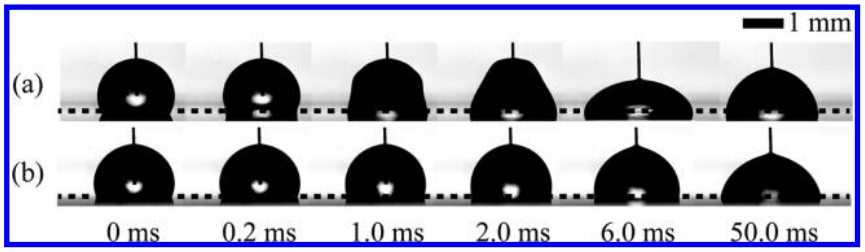

Figure 5. Transient drop deformation of spreading drops with a 5 μL volume for different viscosities at η = 0.56: (a) 1.0 mPa·s and (b) 219.0 mPa·s. The dashed lines indicate the contact surface of the drop.

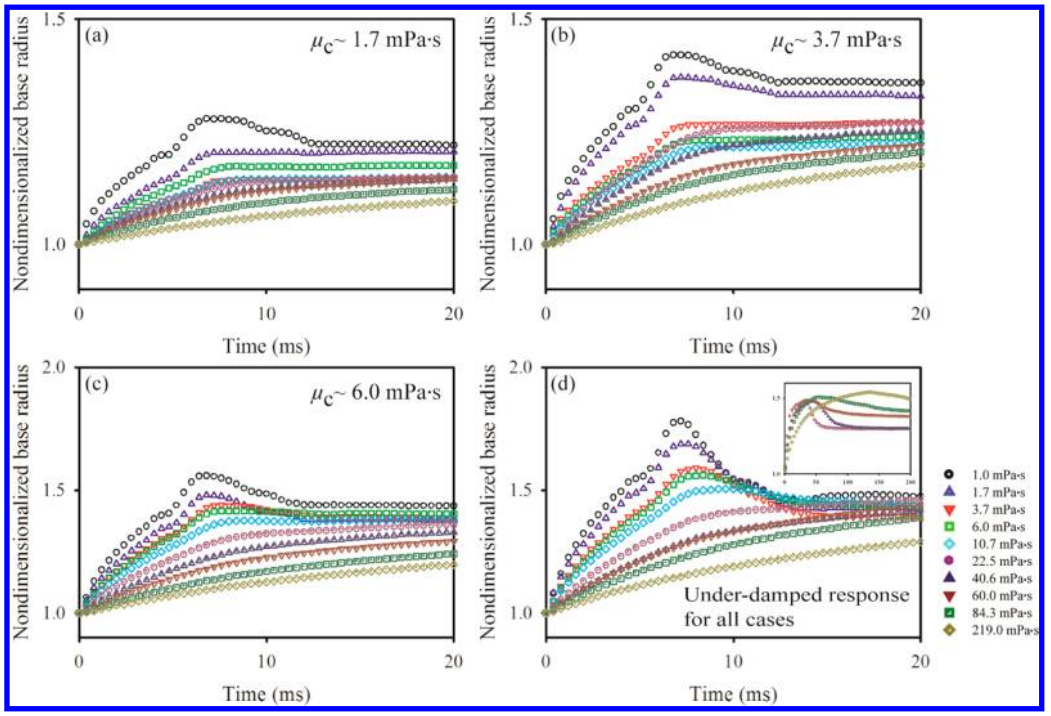

Figure 6. Time evolution of base radius (colored symbols) for spreading drops with a volume of 5 μL at different η: (a) η = 0.25, (b) η = 0.39, (c) η = 0.56, and (d) η = 0.76. Inset: drops with viscosities higher than 22.5 mPa·s spread slowly to a maximum within 200 ms and then slowly retract until they reach an equilibrium state.

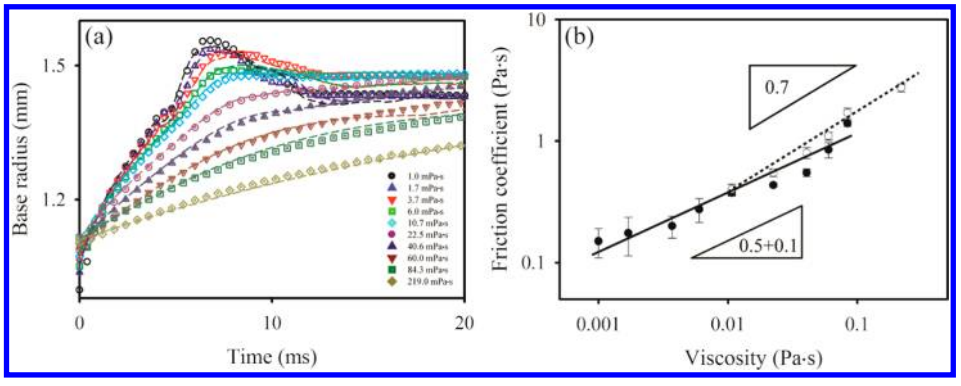

Figure 7. (a) Comparison of the computed time evolution of base radius (lines) with experimental results (symbols) of spreading drops with the volume of 5 μL for various viscosities at η = 0.56. Dashed lines represent computed results using Oh et al.'s model (μ = 1.0−84.3 mPa·s) and Decamps and De Coninck's model (μ = 219 mPa·s). (b) Relationship between viscosity and friction coefficient (log−log scale). Friction coefficients are obtained from fitting the theoretical model to the experimental data. Filled circle and open circle represent friction coefficients obtained from Oh et al.'s model and Decamps and De Coninck's model, respectively.

1.7, 1.7, 3.7, 4.8, and 6.0 mPa·s for η = 0.25, 0.31, 0.39, 0.47, and 0.56, respectively. We found that the critical viscosity increases with η but could not determine the relationship between these parameters. When η is over 0.65, an overdamped response is not observed in experiments although the viscosity is very high (219 mPa·s). In this regime, the drop spreads slowly to a maximum within 200 ms and then slowly retracts until it reaches an equilibrium state (see inset in Figure 6d).

dx.doi.org/10.1021/la401801u | *Langmuir* 2013, 29, 9118−9125

These results will provide helpful information to improve the operation rate of EW-based devices, since the critically damped spreading will be the fastest way for a drop to reach the equilibrium state without the CL oscillation.[2]

We also theoretically explored the effect of drop viscosity on spreading dynamics and compared it to our experimental results (Figure 7a). Our theoretical model (Oh et al.'s model)[20] has some limitations due to the assumption of weak viscous flow. Thus, we used the model of Decamps and De Coninck[18] in the high viscosity regime. They assumed that drop volume was conserved and that the drop shape retained a spherical cap during the spreading process. Thus, the base radius was $R = (3\Delta/\pi)^{1/3} \sin\theta(2 - 3\cos\theta + \cos^3\theta)^{-1/3}$ and this was applied to the molecular kinetic theory considering the EW effect, $dR/dt = \lambda^{-1}\gamma(\cos\theta_Y + \eta - \cos\theta)$, where λ denotes the friction coefficient. However, this model did not consider viscous dissipation and CAH. Spreading behaviors are predicted accurately by Oh et al.'s model up to a drop viscosity of 84.3 mPa·s. On the other hand, Decamps and De Coninck can successfully predict the spreading behavior of drops with viscosity ranging from 10.7 to 219 mPa·s. By fitting these theoretical models to our experimental results, we obtained the friction coefficient and found that the coefficient has a logarithmically linear relationship with drop viscosity in the low and high viscosity regimes, and a slight transition in between these regimes (Figure 7b). Oh et al.'s model and Decamps and De Coninck's model are, respectively, proportional to the 0.5 + 0.1th and 0.7th powers of viscosity. This slight difference is because Oh et al.'s model independently considers viscous dissipation, CL friction, and pinning force; on the other hand, Decamps and De Coninck's model considers only CL friction. Thus, the friction coefficients obtained by Decamps and De Coninck's model include the viscous dissipation and pinning force together with CL friction. Consequently, Oh et al.'s model is believed to predict the dependence of viscosity on friction coefficient better than Decamps and De Coninck's model.

We found experimentally that the maximum velocity (per η) has a power-law dependence on viscosity, $U_{max}/\eta \propto \mu^{-0.3}$ (Figure 8). The slight change in surface tension corresponding to that of viscosity does not affect this power-law. From the balance between the CL friction (λU) and electrical force (F_e) at the early stages, we could determine that the maximum velocity per electrical force (or η) was inversely proportional to the frictional coefficient. Thus, drop viscosity has a weak effect on maximum velocity rather than CL friction at the early stages.

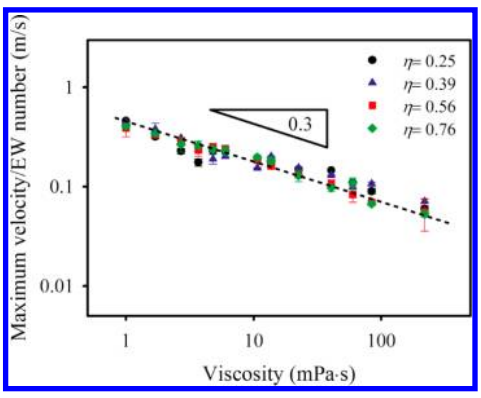

Figure 8. Effect of the drop viscosity on the maximum velocity (per η) (log–log scale).

Also, we found that viscosity rarely has an influence on the time to reach the maximum velocity (0.2–0.4 ms).

4. CONCLUSIONS

We investigated the effects of drop size and viscosity on spreading dynamics driven by DC EW. In order to quantify these effects on the spreading process, the base radii of spreading drops were measured. By fitting the theoretical model to experimental results, we obtained the friction coefficient and found that it was hardly varied by drop size and applied voltage. An empirical relationship was established, that both switching time and settling time are proportional to 1.5th power of the effective base radius; this could also be derived from a theoretical model. We determined that the maximum velocity is proportional to the square of applied voltage. Experiments show a distinct transition in spreading pattern when the viscosity of a drop is varied. We obtained the critical viscosity for the change in spreading patterns with respect to η and found that critical viscosity increases as η increases. At high η (>0.65), an overdamped oscillation was not observed in experiments, even if the viscosity was very high (219 mPa·s). By fitting the theoretical models to experimental results, we obtained the friction coefficient, and first found that the friction coefficient is nearly proportional to 0.6th power of viscosity and has weak dependence on applied voltage and drop size. Finally, a weak dependence of the maximum velocity on drop viscosity was found. To summarize, we explored the effects of each force acting on spreading dynamics by varying factors such as drop size, viscosity, and applied voltage, and found the relationships between these factors and the representative characteristics of spreading dynamics, such as response time and speed. In addition, CL friction was estimated and its relation to the above factors was identified by using theoretical models. This work will provide helpful information in the designing of EW-based devices when physical properties (e.g., viscosity and drop size) and applied voltage are varied to meet their requirements.

■ ASSOCIATED CONTENT

Supporting Information

Voltage dependence of the apparent contact angle for drops with different sizes. Drop size and applied voltage dependence of the friction coefficient. This material is available free of charge via the Internet at http://pubs.acs.org.

■ AUTHOR INFORMATION

Corresponding Author

*(I.S.K.) Phone: +82-54-279-2273. Fax: +82-54-279-2699. E-mail: iskang@postech.ac.kr. (J.M.O.) Phone: +82-54-279-2952. Fax: +82-54-279-2699. E-mail: jmo0902@postech.ac.kr.

Notes

The authors declare no competing financial interest.

■ ACKNOWLEDGMENTS

This work was supported by the National Research Foundation of Korea (NRF) Grant No. R0A-2007-000-20098-0 funded by the Korea government (MEST) and No. 20090083510 through Multiphenomena CFD Engineering Research Center. We thank Dr. S. H. Lee and Mr. J. S. Yoon at Femtofab for helpful assistance.

REFERENCES

(1) Cho, S. K.; Moon, H.; Kim, C.-J. Creating, transporting, cutting, and merging liquid droplets by electrowetting-based actuation for digital microfluidic circuits. *J. Microelectromech. Syst.* **2003**, *12*, 70−80.

(2) Kuiper, S.; Hendriks, B. H. W. Variable-focus liquid lens for miniature cameras. *Appl. Phys. Lett.* **2004**, *85*, 1128−1130.

(3) Sen, P.; Kim, C.-J. A fast liquid-metal droplet switch using EWOD. *IEEE 20th International Conference on MEMS*, 2007, Kobe, Japan, pp 767−770.

(4) Heikenfeld, J.; Steckl, A. J. High-transmission electrowetting light valves. *Appl. Phys. Lett.* **2005**, *86*, 151121.

(5) Hou, L.; Smith, N. R.; Heikenfeld, J. Electrowetting manipulation of an optical film. *Appl. Phys. Lett.* **2007**, *90*, 251114.

(6) Hayes, R. A.; Feenstra, B. J. Video-speed electronic paper based on electrowetting. *Nature* **2003**, *425*, 383−385.

(7) Mugele, F. Fundamental challenges in electrowetting: From equilibrium shapes to contact angle saturation and drop dynamics. *Soft Matter* **2009**, *5*, 3377−3384.

(8) Blake, T. D. The physics of moving wetting lines. *J. Colloid Interface Sci.* **2006**, *299*, 1−13.

(9) Blake, T. D.; Clarke, A.; Statterfield, E. H. An investigation of electrostatic assist in dynamic wetting. *Langmuir* **2000**, *16*, 2928−2935.

(10) Bonn, D.; Eggers, J.; Indekeu, J.; Meunier, J.; Rolley, E. Wetting and spreading. *Rev. Mod. Phys.* **2009**, *81*, 739−805.

(11) Smith, N. R.; Hou, L.; Zhang, J.; Heikenfeld, J. Experimental validation of >1 kHz electrowetting modulation. *17th Biennial University/Government/Industry Micro/Nano Symposium*, 2008, Louisville, Kentucky, pp 11−14.

(12) Dash, S.; Kumari, N.; Garimella, S. V. Frequency-dependent transient response of an oscillating electrically actuated droplet. *J. Micromech. Microeng.* **2012**, *22*, 075004.

(13) Sen, P.; Kim, C.-J. Capillary spreading dynamics of electrowetted sessile droplets in air. *Langmuir* **2009**, *25*, 4302−4305.

(14) Annapragada, S. R.; Dash, S.; Garimella, S. V.; Murthy, J. Y. Dynamics of droplet motion under electrowetting actuation. *Langmuir* **2011**, *21*, 8198−8204.

(15) Ren, H.; Fair, R. B.; Pollack, M. G.; Shaughnessy, E. J. Dynamics of electro-wetting droplet transport. *Sens. Actuators, B* **2002**, *87*, 201−206.

(16) Bavière, R.; Boutet, J.; Fouillet, Y. Dynamics of droplet transport induced by electrowetting actuation. *Microfluid. Nanofluid.* **2007**, *4*, 287−294.

(17) Roques-Carmes, T.; Hayes, R. A.; Feenstra, B. J.; Schlangen, L. J. M. Liquid behavior inside a reflective display pixel based on electrowetting. *J. Appl. Phys.* **2004**, *95*, 4389−4396.

(18) Decamps, C.; De Coninck, J. Dynamics of spontaneous spreading under electrowetting conditions. *Langmuir* **2000**, *16*, 10150−10153.

(19) Wang, K.-L.; Jones, T. B. Electrowetting dynamics of microfluidic actuation. *Langmuir* **2005**, *21*, 4211−4217.

(20) Oh, J. M.; Ko, S. H.; Kang, K. H. Analysis of electrowetting-driven spreading of a drop in air. *Phys. Fluids* **2010**, *22*, 032002.

(21) Plesset, M. S. On the stability of fluid flows with spherical symmetry. *J. Appl. Phys.* **1954**, *25*, 96−98.

(22) Prosperetti, A. Viscous effects on perturbed spherical flows. *Q. Appl. Math.* **1977**, *34*, 339−352.

(23) Plesset, M. S.; Prosperetti, A. Bubble dynamics and cavitation. *Annu. Rev. Fluid Mech.* **1997**, *9*, 145−185.

(24) Walker, S. W.; Shapiro, B.; Nochetto, R. H. Electrowetting with contact line pinning: Computational modeling and comparisons with experiments. *Phys. Fluids* **2009**, *21*, 102103.

(25) Mugele, F.; Baret, J.-C. Electrowetting: From basics to applications. *J. Phys.: Condens. Matter* **2005**, *17*, R705−R774.

(26) Extrand, C. W.; Kumagai, Y. An experimental study of contact angle hysteresis. *J. Colloid Interface Sci.* **1997**, *191*, 378−383.

(27) *CRC Handbook of Chemistry and Physics*, 84th ed.; Lide, D. R., Ed.; Taylor and Francis: Boca Raton, FL, 2007.

(28) *The properties of ordinary water substance*; Dorsey, N. E., Ed.; Reinhold: New York, 1940.

(29) Seborg, D. E.; Edgar, T. F.; Mellichamp, D. A.; Doyle, F. J. *Process dynamics and control*, 2nd ed.; Seborg, D. E., Ed.; Wiley: New York, 2004.